Short-term effects of compaction on soil mechanical properties and pore functions of an Andisol

José Dörner[1,2,*], Sebastián Bravo[1], Marte Stoorvogel[3], Dorota Dec[1,2], Susana Valle[1,2], John Clunes[1,2], Rainer Horn[4], Daniel Uteau[2,5], Ole Wendroth[6], Lorena Lagos[1,2], Felipe Zúñiga[2,7]

[1]Instituto de Ingeniería Agraria y Suelos, Facultad de Ciencias Agrarias y Alimentarias, Universidad Austral de Chile, Valdivia, Chile.

[2]Centro de Investigación en Suelos Volcánicos, Universidad Austral de Chile

[3]Department of Estuarine & Delta Systems, Royal Netherlands Institute for Sea Research (NIOZ), Korringaweg 7, 4401NT Yerseke, The Netherlands

[4]Institute for Plant Nutrition and Soil Science, Christian Albrechts Universität zu Kiel, Hermann Rodewaldstr. 2, 24118 Kiel, Germany

[5]Departament of Soil Science, University of Kassel, Kassel, Germany

[6]Dep. of Plant and Soil Sciences, Univ. of Kentucky, Ag. Sci. North 1100 South Limestone, Lexington, KY 40546

[7]Departamento de Ciencias Naturales y Tecnología, Universidad de Aysén, Eusebio Lillo 630, Coyhaique.

***Email:** josedorner@uach.cl

Keywords: Volcanic ash soils; soil tillage; soil physical quality; field water content; penetration resistance profiles; spatial variability

ABSTRACT

Several studies on soil physical quality have related soil structural properties to bulk density, proposing values for critical limits in relation to the soil compaction status. However, these values are not applicable to Andosols due to their very low bulk density (< 0.9 Mg m^{-3}). This work aimed to evaluate the short-term effects of soil compaction on the soil physical quality of an Andosol. The experiment was established in May 2019. Soil cores were collected from the soil surface and field measurements (penetration resistance, volumetric water content and air conductivity) were conducted to monitor changes in the soil physical quality after compaction events. The soil was compacted using rollers (weighing between 1.20 and 1.37 Mg) to reach three bulk densities (T0: 0.65, T1: 0.75 and T2: 0.85 Mg m^{-3}) by controlling the number of roller passes. Soil compaction induced an increase in the soil bulk density that resulted in an increase in the mechanical strength (e.g. maps of penetration resistance revealed values from (T0) 500 kPa to (T2) 1500 kPa) and caused a decrease in the volume of macropores (e.g. air capacity in T0 and T2 was 22% and 11%, respectively) responsible for water infiltration and flow. The latter provoked an increase in the volumetric water content in the upper 10 cm of the soil, which decreased the field air conductivity due to the reduced pore space and its continuity. Bulk density also increased due to wetting and drying cycles, showing the effect of the natural rearrangement of soil particles, which was more intense in the soil with the lowest bulk density. When the bulk density of the tilled soil increased to values over 0.80 Mg m^{-3}, soil pore functions related to soil aeration reached critical values (air capacity < 10% and air permeability < 1 μm^2) concerning soil compaction, while the soil precompression stress (around 60 kPa) and plant available water (> 20 %) remained within an optimal range.

1. INTRODUCTION

Soil physical degradation due to soil compaction is a major concern worldwide (e.g. Lin and Horn, 2015; Corstanje et al., 2017; Keller et al., 2019) and is considered one of the main threats to sustainable crop production and soil ecological functions (Horn and Fleige, 2003; Lipiec et al., 2012; Shah et al., 2017; Keller et al., 2017, 2019). Several authors (Horn and Fleige, 2003, 2009; Batey, 2009; Keller et al., 2017; Shah et al., 2017) have reported widespread soil compaction problems across large areas of Europe, America, Africa and Australia. Batey (2009) indicated that soil compaction is a soil degradation issue associated not only with agriculture (e.g. animal trampling, trafficking; Reszkowska et al., 2011; Techen et al., 2020), but also with forest harvesting (Solgi et al., 2019), amenity land use (Han et al., 2008), pipeline installation (Batey, 2015; Horn et al., 2021), land restoration (Lal, 2015), wildlife pathways and construction zones in residential and industrial developments. This scenario is complex because high-quality soils are required on a smaller area per capita (Lin and Horn, 2015) in order to satisfy increasing food and energy demands in accordance with sustainable development goals (SDGs), such as goals 2 (Food), 3 (Health), 6 (Water), 13 (Climate) and 15 (Ecosystems) (Bouma, 2019). Therefore, soil compaction must be confronted to avoid the degradation of soils, which is essential not only for food security, but also for other soil functions, including the support of biodiversity, water filtering and storage, and carbon sequestration.

Soil physical quality (SPQ) is a relevant concept to quantify soil degradation issues and to evaluate the impact of management practices on soil functions (Horn and Fleige, 2009; Reynolds et al., 2009; Valle et al., 2018). SPQ is strongly related to soil structure (the spatial arrangement of solids and pore space, with different levels of organization, excluding the chemical variability of solid components; Rabot et al., 2018) and, in turn, to the performance and resilience of the pore system (Horn and Smucker, 2005; Reynolds et al., 2009). The latter underlines the connection between SPQ and the functionality of the porous system. In these terms, high quality soils for agricultural purposes can be defined as those that: i) provide a physical foundation that is strong enough to provide adequate plant support and stable soil structure, but not so strong as to inhibit root proliferation (defined as a penetration resistance < 2 MPa at field capacity), faunal activity (Meurer et al., 2020) and improved nutrient availability, such as nitrogen, over time (Clunes et al., 2021), and ii) offer a continuous pore system that permits good water infiltration, no run-off (e.g. hydraulic conductivity values ≥ 20 cm day^{-1}), good aeration and gas exchange (e.g., air capacity [AC] values $\geq 14\%$), as well as sufficient plant available water (e.g. PAW $> 20\%$) and good workability (Dexter, 2004; Horn and Smucker, 2005; Horn and Fleige, 2009; Reynolds et al., 2009).

Soil bulk density (Bd) is one of the most frequently used SPQ parameters to identify soil compaction (Dec et al., 2008; Valle et al., 2018). Although Bd cannot effectively represent the functionality of the pore system (Bd relates the dry mass of the soil to a defined volume), it is widely used to classify the status of soil compaction because it is relatively easy to measure (Hartge and Horn, 2016). Reynolds et al. (2009) mentioned that for medium to fine-textured soils, an apparent optimal Bd range for maximal crop yield is 0.9 – 1.2 Mg m^{-3}. McQueen and Shepherd (2002) also affirmed that the Bd range presents an upper limit of 1.25 – 1.30 Mg m^{-3}, beyond which crop yield can be reduced by inadequate soil aeration, and a second upper limit of 1.4 – 1.6 Mg m^{-3}, beyond which crop yield can be reduced by excessive mechanical resistance to root elongation (Jones et al., 2003; Drewry et al., 2008). Finally, Reynolds et al. (2009) also sustained that mineral soils with Bd < 0.9 Mg m^{-3} can result in inadequate plant anchoring due to low soil strength, reduced plant-available water, and reduced unsaturated flow of water and dissolved nutrients to plant roots.

Volcanic ash soils (Andisols or Andosols according to USDA or WRB classifications, respectively) cover more than 120 million hectares worldwide (Dahlgren et al., 2004), account for around 1% of the world's soils (Soil Survey Staff, 2010), and present peculiar morphological, physical and chemical properties attributed to the composition of their mineral phase (Matus et al., 2014; Clunes and Pinochet, 2021). The unique characteristics of these soils (detailed below), allow crops to reach potential yields under favorable climatic conditions (Mera et al., 2015; Clunes et al., 2020). The minerals in these soils consist of short-range order materials such as allophane, imogolite, ferrihydrite, Al- and Fe-humus complexes lacking a long-range crystal atomic order (Harsh et al., 2002). Andosols are known for their ability to store large amounts of organic matter because they have great surface areas of non-crystalline constituents that are available for the sorption of organic matter (Matus et al., 2014). The latter implies that Andosols exhibit very low Bd (< 0.9 Mg m^{-3}) and well-defined inter- and intra-aggregate pore systems (Dörner et al., 2010), inducing a sandy behavior near saturation (very high saturated hydraulic conductivity, > 2000 cm d^{-1} according to Dörner et al., 2010) and a large water holding capacity at low matrix potential values (Dörner et al., 2015), influencing water transport under saturated and unsaturated conditions (Dec et al., 2017).

The concept of SPQ has been used in Andosols to quantify the impact of soil tillage and wetting and drying cycles on soil structure dynamics (Dörner et al., 2012) and mechanical strength (Vásquez et al., 2012) and to assess the impact of animal trampling on soil structure dependent properties (e.g. Negron et al., 2019; Dec et al., 2021). Furthermore, Dörner et al. (2013, 2018, 2020) and Valle et al. (2018) have studied the SPQ of different Andosols in southern Chile, concluding that when such soils reached Bd values near 0.9 Mg m^{-3} they must be considered compacted due to very

low AC (< 10%) and air permeability (< 1μm^2). However, due to the complex porosity of these soils, little is known about how an increase in Bd (e.g. due to soil compaction after tillage) affects plant available water (water retained between the field capacity and permanent wilting point), field penetration resistance, air conductivity, and precompression stress. At the same time, few previous studies have combined laboratory analyses with field measurements to assess the short-term effects of compaction on soil physical properties in Andosols. Therefore, the aim of this work was: i) to evaluate the short-term effects of the soil compaction of an Andosol after tillage on soil mechanical strength, volumetric water content and air conductivity measured in the field and ii) to analyze the impact of the Bd increase on the soil precompression stress and soil pore functions and their critical values concerning the soil compaction of a volcanic ash soil. Identifying the short-term effects of soil compaction on the soil physical quality of an Andosol is highly relevant in order to better understand the magnitude and changes in soil functioning as bulk density increases, providing a basis to further analyze the resilience capacity and medium- and long-term changes in the studied soil under field conditions.

2. MATERIALS AND METHODS

2.1 Soils and climatic conditions

This experiment was established at the Universidad Austral de Chile's experimental field station EEAA (Estación Experimental Agropecuaria Austral, 39°46′ S, 73°13′ W, 12 m a.s.l.) in Valdivia, southern Chile, where the average annual temperature is 12 °C with a yearly mean rainfall of 2440 mm between 1901 and 2005 (González-Reyes and Muñoz, 2013). However, rainfall has decreased in the last decade, reaching an annual mean value of 1700 mm (INE, 2020). During 2019, the average temperature reached 11.6 ºC with maximum and minimum values of 25.0º and 3.2º, respectively. In the same year, the annual rainfall was 1816 mm (Figure 1), presenting the highest and lowest values in June (466 mm) and January (15 mm), respectively.

Please insert Figure 1

The evaluated soil is derived from volcanic ashes and is classified as Duric Hapludand (Valdivia Series according to CIREN, 2003) or a Petroduri-Silandic Andosol (WRB, 2006). Topography in the soil series is normally complex, with dominant slopes from 3 to 8%. Bravo et al. (2020) presented the soil horizon distribution after a morphological description of a 200 cm deep soil profile. In the upper 38 cm of this soil, (Ap and B1 horizons) the amount of clay is around 29%, which then decreases to 12% (38 – 57 cm), followed by an increase to 30% (57 – 93 cm, B3 horizon),

and finally decreasing to 10% at the 203 cm depth (2BC horizon). The amount of organic matter varies from 12.7% (Ap horizon) to 2.9% (2BC horizon) and evidence of short-range order minerals was determined in the whole profile with specific dissolution techniques (García-Rodeja et al., 2004). The soil Bd ranged between 0.79 Mg m^{-3} (Ap horizon) and 0.56 Mg m^{-3} (2BC horizon). Detailed information about the studied soil can be also found in Zúñiga et al. (2015), Haas et al. (2018) and Dec et al. (2021).

2.2 Experiment establishment

The agronomic management prior to soil tillage and experiment establishment (end of April) consisted of eliminating the resident natural pasture (about 10 years without management) with two systemic herbicide applications; the second was necessary to eliminate regrowth. Thereafter, traditional ploughing and harrowing (07.05.2019; Figure 2) using offset and tandem discs were conducted, which also allows for the addition of lime and complete fertilization (N, P, K) to achieve a production level of 12 Mg of dry matter (DM) $year^{-1}$ ha^{-1}. The fertilization was used to correct the soil nutrient deficiency and supply the nutrient demands of the pastures (Pinochet, 2011) to reach 12 ppm of P-Olsen and pH_w values of 5.8.

Please insert Figure 2

After soil tillage, the homogenization of all blocks (07.05.2019; Figure 2) was carried out with one pass of a roller from the experimental station (working width: 3m; weight: 1.20 Mg).

2.3 Experiment compaction

The soil was compacted using the roller from the experimental station (described above) and a "Cultivated Land Roller Güttler Mediana 600A" (working width: 6m; weight: 1.37 Mg) to reach three compaction levels which correspond to Bd defined as T0: 0.65, T1: 0.75 and T2: 0.85 Mg m^{-3} (not compacted, compacted and highly compacted, respectively; Figure 2). Plots of 576 m^2 (24 x 24 m) were distributed with 3 blocks for each level of soil compaction (1728 m^2).

The soil compaction levels were achieved by controlling the number of rollers passes (P) before sowing (T0: 1P, T1: 2P, T2: 5P times; 07.05.2019; Figure 2) and after sowing (T0: 1P, T1: 3P, T2: 8P times; 14.05.2019 and 15.05.2019; Figure 2). Finally, soil compaction events (SCE; compaction 1, 2 and 3) were defined by the number of roller passes

and the date on which rollers pass were performed, while M1 indicates field measurements before sowing, M2 after sowing and compaction 1, M3 after compaction 2 and M4 after compaction 3. A diverse pasture was sown including: *L. perenne*, *T. repens*, *F. arundinacea*, *H. lanatus*, *D. glomerata* and *B. valdivianus*.

2.4 Field measurements and soil sampling

To control soil compaction levels, changes in penetration resistance and volumetric water content were measured after soil compaction events (Figure 2). As a reference of compacted soil, we used penetration resistance (PR) values measured in a trampled pasture near the study site where sheep have transited daily for, at least, the last 10 years (Salas et al., 2016). The PR values of the trampled site reached 1663 ± 60 kPa (n = 10). A hand penetrometer (Eijkelkamp, the Netherlands) was used to measure changes in mechanical impedance between depths of 0 – 10 cm (Figure 1). During PR-measurements, the volumetric water content (θ_{Field}, 0-10 cm depth) was measured by using a WET-2-K1 Sensor (Delta-T Devices Ltd., UK). PR was measured in a grid with 96 points distributed across the experiment (12 per treatment, 4 per block).

Mechanical strength profiles were measured on July 5th, 2019 with a Penetrologger (Eijkelkamp, the Netherlands). Considering that the Penetrologger allowed for the measurement of PR values in the soil with an increment depth of 1 cm (between depths of 0-80 cm), the sum of these values (accumulated penetration resistance, APR) was also used to analyze the impact of soil compaction considering the following depths: 0 – 5 cm, 0 – 20 cm and 0 – 60 cm. Soil water content was also registered and the air conductivity was measured in the field by using an Air Permeability PL-300 (UGT GmbH, Germany). All measurements were registered in a grid of 96 points as previously explained.

Regarding soil sampling, stainless cylinders of two volumes were used: 120 cm^3 and 230 cm^3 to determine the consolidation (n = 6) and water retention (n = 7) curves, respectively. To evaluate the consequences of soil compaction on soil physical properties and the changes they induce over time, undisturbed soil samples were collected from the soil surface (0 cm) immediately after soil tillage (07.05.2019, data not shown) and three times after the final roller compaction (15.05.2019, 16.06.2019 and 17.09.2019, see Figure 1) to detect changes in bulk density (Bd), air capacity (AC), plant available water (PAW), air permeability (Ka) and precompression stress (Pc).

2.4 Laboratory Analysis

2.4.1 Water retention curve and derived pore-size distribution

In order to study soil hydraulic properties, the water retention curve and Ka were measured in undisturbed soil samples contained in stainless steel cylinders (v = 230 cm^3; h = 5.60 cm, Ø = 7.20 cm). According to Hartge and Horn (2009), the samples (n = 7) were first carefully saturated from beneath; when saturation was reached, the samples were first weighed, then equilibrated at matric potential values of -1, -2, -3, -6 (with the vacuum method using a sand table), -15, -33 and -50 kPa (with the overpressure method using a pressure chamber) and weighed at each matric potential with an electronic balance (Precisa, 0.01 g accuracy, Switzerland). Sample height was measured at 5 points using a Vernier Caliper (0.01 mm precision). This information was used to correct the volumetric water content due to shrinkage (Dörner et al., 2015). To define the volume of fine pores (FP, Ø < 0.2 μm), disturbed soil samples were air-dried and sieved at 2 mm to be packed in cylinders of 20 cm^3; h = 1.52 cm, Ø = 3.83 cm and then equilibrated at a matric potential of -1543 kPa. The volumes of wide coarse pores (wCP, Ø > 50 μm, which is equivalent to the AC according to Hartge and Horn, 2009) and PAW (Ø > 50 – 0.2 μm) were calculated using the volumetric water contents (θ) measured at different matric potentials in samples used for the water retention curves (Dörner et al., 2015).

2.4.2 Soil precompression stress (Pc)

The soil precompression stress was derived from a consolidation experiment (Hartge and Horn, 2009). Soil samples (n = 6; v = 120 cm^3; h = 3.00 cm, Ø = 7.20 cm) were carefully saturated by capillary rise and thereafter equilibrated at a matric potential of -6 kPa to determine the amount of wide coarse pores and to measure the air conductivity (Kl) of each soil sample using an air-flowmeter (Dörner et al., 2015). Air permeability (Ka) was calculated from Kl (Dörner and Horn, 2006). Thereafter, the following soil mechanical tests were conducted.

The consolidation curve was measured using an oedometer (T-Controls, T3C3, STD 1045) with free drainage. The samples were first stressed by static loading (6, 12, 25, 50, 100, 200 and 400 kPa) for 6 minutes and thereafter, the stresses (σ_n) were removed until 200, 100, 50, 6 and 1 kPa were reached. The soil deformation was measured every 3 minutes during the experiment (0.05 mm accuracy). The precompression stress (Pc, defined by Horn and Fleige (2009) was defined in accordance with Casagrande (1936) using the mathematical methodology proposed in Baumgartl and Köck (2004).

After the aforementioned analysis, the samples were weighed and air permeability was measured. These were then dried at 105 ºC for 24 hours to define the soil Bd (Hartge and Horn, 2009).

2.4.3 Penetration resistance at the cylinder scale

Before compression test analyses, we used a selection of soil samples collected from the soil surface (0 cm) and 20 cm depths (only collected for this measurement) to measure the penetration resistance at the cylinder scale (PR_{cyl}). A hand-made penetrometer needle with a 30˚cone angle and 3 mm diameter at its thicker end was mounted to a material testing machine (100 kN Allround Table, Zwick/Roell, Ulm, Germany) and pushed into the soil sample at a speed of 0.016 mm s^{-1} up to a depth of 25 mm. The resistance was measured with a 100 N load cell at 0.1 mm intervals and converted to MPa by normalizing the force to the tip area (0.25 cm^2).

2.5 Statistical analyses

The normality of the data was evaluated using the Shapiro-Wilk test ($p \leq 0.05$) and the homogeneity of variance by the Levene test ($p \leq 0.05$). If the data was not normally distributed, it was transformed with the natural logarithm. To analyze the effect of bulk density on measurements conducted in the field (volumetric water content [θ_{Field}], penetration resistance [PR and PR_{cyl}] and accumulated penetration resistance [APR]), a two-way analysis of variance (ANOVA) was performed considering two factors: soil compaction events (SCE) on defined dates (M1 – M4 in Figure 2) and for three different treatments (3 compaction levels: T0, T1 and T2). For the analysis of the physical properties (e.g. Bd, Pc, PAW, AC and Ka), a two-way analysis of variance (ANOVA) was carried out considering two factors: sampling dates (3 dates: 15/05/2019, 15/06/2019 and 17/09/2019) and treatments (3 compaction levels: T0, T1 and T2). If the interaction between factors on the outcome variable was significant, multiple comparisons of means were performed using Tukey contrasts ($p \leq 0.05$) to determine which groups were different. Furthermore, the observed differences between means were tested with Tukey's range test ($p \leq 0.05$). Regression analyses, geostatistical analyses, and penetration resistance profiles were conducted using Sigmaplot v.12, GS+ 5.1.1, and R 4.0.2 (R Core Team, 2020) with RStudio 1.3.1017 (RStudio Team, 2020), respectively.

Regarding spatial changes of physical properties, the following descriptive statistical parameters were calculated: mean, median, maximum, and minimum values, CV, skewness, and kurtosis. The spatial variability structure of the whole area was analyzed with the geostatistical software package GS+ version 9.0. This program defines semivariograms and their respective parameter sets (nugget, Co; sill, Co + C; range, A0). Gaussian, exponential and spherical semivariogram models were used to explain the structure of the spatial variability (i.e. spatial distance within which a soil property behaves similarly; for more details see Nielsen and Wendroth, 2003) of WC, PR / $PR_{0\text{-}20cm}$ / $PR_{0\text{-}$

$_{60cm}$ and $PR_{0\text{-}5cm}$, respectively. Kl-values were transformed to reach a normal distribution, which then facilitated the use of the exponential models. The best mathematical model was chosen based on the highest R^2 and the lowest residual sum of squares. The degree of dependence was calculated via the ratio nugget/sill, as proposed by Cambardella et al. (1994). More details regarding geostatistical analyses can be found in Nielsen and Wendroth (2003).

3. RESULTS

3.1 Changes in Andosol's physical properties during experiment establishment

Figure 3 presents a sequence of field measurements (PR and field volumetric water content) conducted before and after compaction events (Figure 2). PR values measured in the same soil under an intensively grazed pasture (1.6 MPa, red line) and directly after soil tillage (0.7 MPa, blue line) are included as references to quantify the effect of roller passes on soil mechanical strength. As the number of soil compaction events increased, the PR increased across treatments, even exceeding the PR values registered in the intensively grazed pasture. This significant increase due to the compaction events was observed in T2 ($p < 0.01$). Similar results were observed for the field volumetric water content (θ_{Field}), which increased on average by 5% ($p < 0.001$) in the treatment with the highest Bd (T2; $p < 0.01$) as a result of the second soil compaction event (registered in M2).

Please insert Figure 3

3.2 Field spatial changes in soil penetration resistance, volumetric water content and air conductivity after experiment establishment

Field measurements were conducted on July 5th, 2019 to identify the effect of soil compaction on soil mechanical strength and pore functions (Table 1). While field soil water content presented values ranging between 32 and 61% (CV: 12%), PR and air conductivity (Kl) varied between 0.2 and 1.5 MPa (CV 42%) and 0.03 and 17.6 cm s^{-1} (CV: 148%), respectively. As expected, the sum of PR values increased as the thickness of the considered soil layer increased; however, the proportion between registered max and min values decreased, as was also observed for CV (0 – 5 cm: 7.8 / 35%; 0 – 20 cm: 2.7 / 15%; 0 – 60 cm: 1.6 / 11).

Please insert Table 1

The dependence degree (DD) of all of the properties presented values between 24 and 38, with range (A) values between 90 and 303 m (Table 2).

Please insert Table 2

The spatial variability of physical properties measured in the field is presented in Figure 4. A well-defined gradient of increasing PR throughout the experiment was observed, which coincides with the increase in the expected Bd (from 0.65 till 0.85 Mg m^{-3}) reached after soil compaction events. While the volumetric water content increased in the same way (from T0 to T2), the opposite was observed in the air conductivity measured in the field.

Please insert Figure 4

When considering the sum of PR values (Figure 5), the well-defined gradients identified at the 10 cm depth (Figure 3) can be clearly observed at $PR_{0\text{-}5cm}$ and $PR_{0\text{-}20cm}$, although they tend to disappear at $PR_{0\text{-}60cm}$. The highest sum of PR values was observed in T2, while the lowest were assessed in T0.

Please insert Figure 5

To evaluate PR as a function of soil depth, PR profiles at two different scales are presented in Figure 6. PR profiles considered changes registered at the cm scale (Penetrologger till the 80 cm depth; Figure 6A), and the mm scale (in soil samples with a 3 cm height, PR_{cyl}; Figure 6B). The PR values observed in the first 0–10 cm of soil depth presented the following tendency: T2 > T1 > T0; however, these differences disappeared when the 20 cm soil depth was reached.

The highest PR values were registered between the 20–30 cm depth (between 1.5 – 1.7 MPa). Afterwards, they decreased with increasing soil depth, reaching values around 1.0 MPa.

A well-defined increase of PR_{cyl} was identified at the mm scale; the mechanical strength reached max values till the 12 mm depth and then decreased. In the first soil layer (0–3 cm), PR_{cyl} behaved as follows: T2 > T1 > T0, reflecting the presence of a platy structure as identified in the field at T2 (Figure 6C). These differences in the second soil layer (20–23 cm) tended to disappear at greater depths (Figure 6C). Accumulated penetration resistance (APR) differed between treatments evaluated at the same depth ($p < 0.001$), following the same order T2 > T1 > T0 (Figure 6D). At the 0–5 cm depth, T2 was 5.9 MPa, while T0 and T1 only reached a mean of 3.2 and 4.6 MPa, respectively. The APR at 0–20 cm for T2, T1 and T0 was 29.3, 27.3 and 23.9 MPa, respectively. Finally, the accumulative effect of penetration resistance in each treatment was higher at 0–60 cm, reaching values of 80.1, 75.8 and 69.4 MPa for T2, T1 and T0, respectively ($p < 0.001$).

Please insert Figure 6

3.3 Temporal changes in soil physical properties

The soil compaction effect can be observed in the measurements conducted in May 2019 (Figure 7). The differences in Bd observed in May 2019 (T2 > T1 > T0; $p < 0.001$) disappeared in June 2019 due to an increase of Bd in T0 and T1, while T2 did not change. The opposite tendency was observed in AC from May 2019 (T0 > T1 > T2) to September 2019: T0 > T2 > T1; however, similar to the two previous parameters, the factors showed a significant interaction ($p < 0.001$). On the contrary, no differences were observed between PAW values over time (May-June-September 2019), but a slight difference ($p < 0.05$) was observed between T1 and T0 in September. Air permeability before the consolidation experiment (Ka BCE) was consistent with changes among treatments: T0> T1 = T2 ($p < 0.01$). Furthermore, a recuperation of Ka BCE was observed from June 2019 to September 2019 ($p < 0.001$). The latter was also observed after the consolidation experiment ($p < 0.001$), with Ka AFE reaching its highest value in September 2019. However, no differences were observed between treatments for Ka AFE during the time evaluated ($p > 0.05$).

Please insert Figure 7

Figure 8 relates SPQ parameters to Bd. Pc increased exponentially with the rise in Bd ($p < 0.0001$), with Pc values considered as very low (< 30 kPa), and then increasing to those pondered as mean (60–90 kPa). On the other hand, the increase in Bd implied an increase in PAW ($p < 0.05$), though a decrease in AC ($p < 0.0001$) and Ka ($p < 0.0001$) was recorded. With higher Bd-values (> 0.8 Mg m^{-3}), both AC and Ka reached critical values concerning soil compaction, while PAW values remained > 20%.

Please insert Figure 8

Finally, as the AC increased, the volume of PAW decreased ($p < 0.001$, Figure 9). This increase in the volume of macropores induced not only an increase in Ka ($p < 0.001$) but a significant decrease in soil Pc, which can be defined as very low. Along with the lowest AC-values (< 10%), Ka reached critical values concerning soil aeration, though Pc-values did not reach levels considered as high.

Please insert Figure 9

4. DISCUSSION

4.1 Short-term effects of soil compaction on the physical quality of a volcanic ash soil after tillage

Soil compaction occurs during agricultural activities when the soil is subjected to mechanical stresses that exceed its Pc, resulting in irreversible soil structure degradation (Horn, 1988). This "static loading concept" of soil compaction has expanded in recent years because the use of cyclic loading experiments has allowed us to understand that even when soils are exposed to repeated (as occurs during soil compaction events conducted in the present experiment) loads lower than Pc, a significant soil deformation takes place (Peth and Horn, 2006; Peth et al., 2010, Gubianni et al., 2018; Dörner et al., 2020; Dec et al., 2021) due to the weakening effect of standing water. Therefore, as occurred in our experiment, soil compaction events lead to a densification of soils in the short-term that negatively affect i) soil mechanical strength (e.g. see Figure 6) and form a platy soil structure, in addition to root growth due to an increase in penetration resistance (observed by Lipiec and Hatano (2003) and Dec et al. (2021)), ii) pore-size distribution and pore

functions (e.g. a decrease in air conductivity in Figure 8 as also observed by Schjønning and Rasmussen (2000), Simojoki et al. (2008)), and iii) transport processes in soils (e.g. the effect of soil compaction on water table dynamics of Aquands (Dörner et al., 2017)). This study found that when a volcanic ash soil reached bulk density values (due to soil tillage and soil compaction events) near those defined as "Andic Property" (0.9 Mg m^{-3}) they presented critical values of air capacity (< 10 %) and air permeability (< 1μm^2) concerning soil aereation problems in the short-term, similar to highly dense soils (Horn and Fleige, 2009; Reynolds et al., 2009). These critical values reveal that aereation problems occurred in mineral soils when bulk density values were between 1.25 – 1.30 Mg m^{-3} (McQueen and Shepherd, 2002), which highlights the peculiar behavior of volcanic ash soils.

Soil tillage breaks aggregates and decreases contact points and areas between them, reducing the soil mechanical strength (Figure 3). During this experiment, the roller passes applied new stresses (as cyclic loading events) to the tilled soil, which resulted in increased contact areas between aggregates and Bd. The soil mechanical strength increased and a platy soil structure was formed in T2 as a response to the repeated applied loads (see APR and platy structure in Figure 6). At the same time, even when no load was applied in T0 after the last compaction event, a natural rearrangement of soil particles/aggregates occurred in this treatment, which increased the contact areas between aggregates, Bd and the mechanical strength (see increases in Bd and Pc in the first two sampling dates in Figure 7), most likely as a response to wetting and drying (WD) cycles (see dynamics of rainfalls and air temperature in Figure 1), as also assessed in aggregate beds of volcanic ash soils by Seguel and Horn (2006). Soil structural changes, because of both external (soil compaction events) and internal (wetting and drying cycles) stresses, reduced the total porosity and increased the water retained in the soil as assessed in the field (Figure 2) due to a reduction of macropores (AC, see Figure 7) and an increase in PAW (Figure 9), as was also assessed in a Typic Hapludand after soil tillage (Dörner et al., 2012).

The first two soil sampling events allowed us to assess the short-term effects after one month of pasture establishment and soil compaction and, therefore, provide a basis for a medium- and long-term analyses. As the Bd increased due to compaction events, the soil reached a soil mechanical strength that reduced the WD cycle-dependent changes in soil structure, such as those observed in T0 and T1 (e.g. while Bd in T0 increased from 0.64 to 0.78 Mg m^{-3} between two first soil samplings, in T2 it remained at 0.82 Mg m^{-3}). Later (soil sampling conducted in September), further dynamic changes in soil structure were evidenced e.g., an increase in AC, and Ka, while the PAW did not change significantly.

The effects of soil compaction on SPQ are generally assessed with classic soil sampling and measurements that are time-consuming and labor-intensive. Despite these disadvantages, these procedures permit a better understanding of soil deformation-dependent processes in soil systems as evidenced by Peth and Horn (2006), Gubiani et al. (2018) and Dörner et al. (2020) who studied the effect of cyclic loading on soil deformation processes in different soils. Nonetheless, as was carried out in the present study, the use of field measurements that combine the quantification of mechanical strength, field volumetric water content and air conductivity provide basic, yet highly relevant information to analyze the effects of tillage (e.g. Figure 3 and 4), grazing and irrigation managements on soil/pasture/animal systems (Dec et al., 2021). The results of the conducted trial show that the combination of field and labororatory measurements allowed us to achieve a better understanding of e.g. i) how the mechanical strength changed after roller passings (Figure 3), ii) how this compaction reduced the air conductivity of the soil (Figure 4), and iii) to what magnitude soil structure dependent properties varied over time (Figure 7). This methodology identified a compaction-dependent increase in PR and the associated formation of a platy soil structure (Figure 6), which was also related to a decrease in air conductivity (Figure 4) and air capacity (Figure 7), but not to a decrease in PAW ($p > 0.05$).

Finally, the spatial distribution analysis helped us to describe the spatial behavior of soil Bd and its spatial relationship with other properties, manifested in zones with higher Bd (> 0.8 Mg m^{-3}), coinciding with those of higher volumetric water content (> 55 Vol. %) and lower air conductivity (< 0.7 log cm s^{-1}). Our analyses revealed that phenomena were not spatially random, but were identified as spatially representative observations including distances over which these processes coincide. Mzuku et al. (2005) mentioned that the spatial variability of soil properties across the field can be used to explain the variability between site-specific management zones based on their measured soil physical properties. This approach is critical for the success of site-specific management in order to improve the efficient use of natural resources (e.g., Wendroth et al., 2001). In these terms, the use of classical statistics (Figure 8 and 9), along with spatial statistics (Figure 4 and 5), helped us to better understand the effects of soil compaction on soil physical properties across the field and their common scales of variation (Nielsen and Wendroth, 2003).

4.2 Bulk density as a parameter to quantify SPQ changes after tillage of a volcanic ash soil

After soil compaction, the dry Bd values shifted to a range between 0.80 and 0.85 Mg m^{-3}. The latter means that: i) the penetration resistance measured after experiment establishment in T2 reached values comparable to the same soil under an intensively grazed pasture (Figure 3), ii) a redistribution of the pore system took place, which is reflected in a

decrease in AC (reaching critical values concerning gas exchange) and an increase in PAW (Figure 8 and 9) and iii) the amount of water retained in the pore system increased, causing the air conductivity to decrease (Figure 4). Dörner et al. (2013) studied the same soil series under different land uses (less intensive: soil under native forest; medium intensive: recently seeded pasture without grazing and highly intensively used soil: pastures under winter grazing) and found that bulk densities ranged between 0.55 Mg m^{-3} and 0.73 Mg m^{-3}. They concluded that the AC of the soil was the highest under the least intensive soil management (e.g. soil under native forest had values higher than 14%, similar to those assessed in the treatment with the lowest Bd in this study); however, critical values concerning soil compaction could be reached as a result of soil structure degradation due to soil tillage and intensive grazing. In a shallow volcanic ash soil under naturalized grassland and secondary native forest, Dörner et al. (2017) registered Bd values ranging from 0.15 to 0.65 Mg m^{-3} and concluded that when this maximal Bd was reached, soil compaction problems related to poor air exchange occurred.

As stated in the present study, we cannot use only the Bd of the soil to assess potential soil physical degradation after soil compaction events over a tilled soil, i.e. we must relate changes in Bd to soil physical properties relevant for root exploration (Pc), soil aeration (AC, Ka), water holding capacity (PAW) and go further, in order to understand and explain the physical quality of Andosols through indicators of physical interactions. Provided that pores responsible for gas exchange (AC) are very sensitive to soil deformation when the soil is exposed to external (soil compaction, e.g. Gebhardt et al., 2009) or internal forces (soil shrinkage, e.g. Dörner et al., 2011), they reflect the dynamic behavior of the soil structure (Dörner et al., 2012). A decrease in AC denotes soil structure degradation, which also means a decrease in the air flow registered in the field (Figure 4) and the lab (Figure 9; Ka at AC values lower than 10% reached values < 1μm^2). On the other hand, as the AC increased, Pc decreased exponentially, reflecting the loss in soil mechanical strength. Finally, although it is true that the highest Bd values reached after soil compaction (0.80 – 0.85 Mg m^{-3}) were related to restrictions in soil aeration, we must point out that these relationships derived from samples collected from a short-term experiment over tilled soil. In these terms, the well-known resilience capacity of these soils, and soil aggregation effects (Zúñiga et al., 2015) must be validated in further studies to better assess the SPQ of volcanic ash soils and their critical values.

CONCLUSIONS

The short-term effects of the soil compaction of an Andosol during tillage induced an increase in contact areas between aggregates that was evidenced by the platy structure formation in the highly compacted soil. The increase in soil bulk density after compaction resulted in an increase in mechanical strength at different scales and a decrease in the volume of macropores (air capacity) responsible for water infiltration. The latter provoked an increase in field volumetric water content in the upper 10 cm of the soil, which decreased the field air conductivity.

The bulk density increased not only due to mechanical stresses, but also as a consequence of wetting and drying cycles. Even when no load was applied (between M2 and M3), a natural rearrangement of soil particles/aggregates occurred in T0, which increased the bulk density and mechanical strength.

When the bulk density of the tilled soil increased to values over 0.8 Mgm^{-3}, soil pore functions related to soil aeration reached critical values concerning soil compaction. The arrangement of aggregates after compaction also induced an increase in soil precompression stress and the plant available water remained within an optimal range.

Finally, the results of the present study show that the combination of field and laboratory measurements provide a better understanding of the deformation processes after soil compaction and how they affect air transport processes, increased mechanical strength and plant available water, i.e. an increase in bulk density after tillage and compaction is related to a decrease in field air conductivity.

ACKNOWLEDGMENTS

We would like to thank the FONDECYT Grant 1191057 for funding this research project. Dr. José Dörner and Dr. Felipe Zúñiga thank the Alexander von Humboldt Foundation for the Grant “Georg Foster Fellowship for Experienced Researchers”, which allowed a renewed research stay in the framework of an Alumni Sponsorship 2019 at the Christian Albrechts University in Kiel and the University of Kassel (Germany). José and Felipe are grateful for the hospitality and friendship of their colleagues in Kiel and Kassel. Finally, the authors are grateful for the field and laboratory work conducted by Mónica Díaz, Victor Vera Peters, Belén Henríquez, Tomás Macías and the Project Team.

REFERENCES

Batey, T., 2009. Soil compaction and soil management–a review. Soil Use Manage. 25(4), 335–345. https://doi.org/10.1111/j.1475-2743.2009.00236.x

Batey, T., 2015. The installation of underground pipelines: effects on soil properties. Soil Use Manage. 31, 60–66. https://doi.org/10.1111/sum.12163

Baumgartl, T., Köck, B., 2004. Modeling volume change and mechanical properties with hydraulic models. Soil Sci. Soc. Am. J. 68, 57–65. https://doi.org/10.2136/sssaj2004.5700

Bouma, J., 2019. Soil security in sustainable development. Soil Syst. 3(1), 5. https://doi.org/10.3390/soilsystems3010005

Bravo, S, González-Chang, M., Dec, D., Valle. S., Wendroth, O., Zúñiga, F., Dörner, J., 2020. Using wavelet analyses to identify temporal coherence in soil physical properties in a volcanic ash-derived soil. Agr. Forest. Meteorol. 285–286,107909. https://doi.org/10.1016/j.agrformet.2020.107909

Cambardella, C.A., Moorman, T.B., Parkin, T.B., Karlen, D.L., Novak, J.M., Turco, R.F., Konopka, A.E., 1994. Field-scale variability of soil properties in central Iowa soils.

Casagrande, A., 1936. Characteristics of cohesive soils affecting the stability of slopes and Earth fill. J. Boston Soc. Civil Eng. 23, 13–32.

CIREN (Centro de Información de Recursos Naturales), 2003. Descripciones de Suelos. Materiales y Símbolos. Estudio Agrológico X Región. CIREN, Publicación 123, Santiago.

Corstanje, R., Mercer, T.G., Rickson, J.R., Deeks, L.K., Newell-Price, P., Holman, I., Kechavarsi, C. Waine, T.W., 2017. Physical soil quality indicators for monitoring British soils. Solid Earth 8(5), 1003–1016. https://doi.org/10.5194/se-8-1003-2017

Clunes, J., Pinochet, D., 2020. Effect of slow-release nitrogen on the nitrogen availability in an andisol and the critical nitrogen concentration in wheat. Agronomy Journal, 112(2), 1250–1262. https://doi.org/10.1002/agj2.20131

Clunes, J., Pinochet, D., 2021. Leucine retention by the clay-sized mineral fraction. An indicator of C storage. Agro Sur 48(3), 37–46. https://doi.org/10.4206/agrosur.2020.v48n3-05

Clunes, J., Dörner, J., Pinochet, D., 2021. How does the functionality of the pore system affects inorganic nitrogen storage in volcanic ash soils?. Soil Till. Res. 205, 104802. https://doi.org/10.1016/j.still.2020.104802

Dahlgren, R.A., Saigusa, M., Ugolini, F.C., 2004. The nature, properties and management of volcanic soils. Adv. Agron. 82(3), 113–182.

Dec, D., Dörner, J., Bekcer-Fazekas, O., Horn, R., 2008. Effect of bulk density on hydraulic properties of homogenized and structured soils. J. Soil Sc. Plant Nutr. (1):1-13.

Dec, D., Zúniga, F., Thiers, O., Paulino, L., Valle, S., Villagra, V., Tadich, I., Horn, R., Dörner, J., 2017. Water and temperature dynamics of Aquands under different uses in southern Chile. J. Soil Sci. Plant Nutr. 17(1), 141–154. http://dx.doi.org/10.4067/S0718-95162017005000011

Dec, D., Bravo, S., Horn, R., Uteau, D., Peth, S., Zúñiga, F., Clunes, J., Granda, S., Martínez, Ó., Balocchi Ó., Alonso, M., 2021. Analyzing the impact of grazing and short-term irrigation management on soil mechanical strength of a volcanic ash soil under different types of pastures. Soil Till. Res. 213, 105130. https://doi.org/10.1016/j.still.2021.105130

Dexter, A. R., 2004. Soil physical quality: Part II. Friability, tillage, tilth and hard-setting. Geoderma 120(3-4), 215–225. https://doi.org/10.1016/j.geoderma.2003.09.005

Dörner, J., Horn, R., 2006. Anisotropy of pore functions in structured Stagnic Luvisols in the weichselian moraine region in N Germany. J. Plant Nutr. Soil Sci. 169, 213–220. https://doi.org/10.1002/jpln.200521844

Dörner, J., Dec, D., Peng, X., Horn, R., 2010. Effect of land use change on the dynamic behaviour of structural properties of an Andisol in southern Chile under saturated and unsaturated hydraulic conditions. Geoderma 159,189–197. https://doi.org/10.1016/j.geoderma.2010.07.011

Dörner, J., Dec, D., Zúñiga, F., Sandoval, P., Horn, R., 2011. Effect of the land use change on Andosol's pore functions and their functional resilience after mechanical and hydraulic stresses. Soil Till. Res. 115-116, 71–79. https://doi.org/10.1016/j.still.2011.07.002

Dörner, J., Dec, D., Feest, E., Vásquez, N., Díaz, M., 2012. Dynamics of soil structure and pore functions of a volcanic ash soil under tillage. Soil Till. Res. 125, 52–60. https://doi.org/10.1016/j.still.2012.05.019

Dörner, J., Dec, D., Zúñiga, F., Horn, R., López, I., Leiva, C., Cuevas, J. 2013. Soil Changes in the Physical Quality of an Andosol under Different Management Intensities in Southern Chile. In: Krümmelben, J., Horn, R., Pagliai, M. (Eds.), Soil Degradation. Advances in Geoecology 42, Catena Verlag GMBH Reiskirchen, Germany, pp. 262–281.

Dörner, J., Huertas, J., Cuevas, J.G., Leiva, C., Paulino, L., Arumí, J.L., 2015. Water content dynamics in a volcanic ash soil slope in southern Chile. J. Plant Nutr. Soil Sci. 178 (4), 693–702. https://doi.org/10.1002/jpln.201500112

Dörner, J., Horn, R., Dec, D., Wendroth, O., Fleige, H., Zúñiga, F., 2017. Land use dependent change of soil mechanical strength and resilience of a shallow volcanic ash soil in southern Chile. Soil Sci. Soc. Am. J. 81, 1064–1073. https://doi.org/10.2136/sssaj2016.11.0378

Dörner, J., Dec, D., Matus, F., Zúñiga, F., Ordóñez, I., Horn, R., 2018. The relevance of soil structure conservation and carbon sequestration in Chilean volcanic ash soils for achieving sustainable development goals. In: Lal, R., Horn, R., Kosaki, T. (Eds.). Soil and Sustainable Development Goals. GeoEcology Essay, Catena Soil Sciences Stuttgart: ISBN 978-3-510-65425-3, pp. 118–125.

Dörner, J., Horn, R., Uteau, D., Rostek, J., Zúñiga, F., Peth, S., Dec, D., Fleige, H., 2020. Studying the soil pore physical resistance and resilience of a shallow volcanic ash soil subjected to pure cyclic loading. Soil Till. Res. 204, 104709. https://doi.org/10.1016/j.still.2020.104709

Drewry, J.J., Cameron, K.C., Buchan, G.D., 2008. Pasture yield and soil physical property responses to soil compaction from treading and grazing—a review. Soil Res. 46(3), 237–256. https://doi.org/10.1071/SR07125

Garcıa-Rodeja, E., Nóvoa, J.C., Pontevedra, X., Martınez-Cortizas, A., Buurman, P., 2004) Aluminium fractionation of European volcanic soils by selective dissolution techniques. Catena 56(1-3), 155–183. https://doi.org/10.1016/j.catena.2003.10.009

Gebhardt, S., Fleige, H., Horn, R., 2009. Effect of compaction on pore functions of soils in a Saalean moraine landscape in North Germany. J. Plant Nutr. Soil Sci. 172(5), 688–695. https://doi.org/10.1002/jpln.200800073

Gonzales-Reyes, A., Muñoz, A.A., 2013. Cambios en la precipitación de la ciudad de Valdivia (Chile) durante los últimos 150 años. Bosque 34(2), 191–200.

Gubiani, P.I., Pértile P., Reichert, J.M., 2018. Relationship of precompression stress with elasticity and plasticity indexes from uniaxial cyclic loading test. Soil Till. Res. 180, 29–37. https://doi.org/10.1016/j.still.2018.02.004

Han, L.B., Song, G.L., Zhang, X., 2008. Preliminary observations on physiological responses of three turfgrass species to traffic stress. Horttechnology, 18, 139–143. https://doi.org/10.21273/HORTTECH.18.1.139

Hartge, R., Horn, R., 2009. Die physikalische Untersuchung von Böden. Praxis Messmethoden Auswertung. 4. vollst. Überarbeitete Auflage. Schweizerbart Vorlage, Stuttgart.

Harsh, J., Chorover, J., Nizeyimana, E., 2002. Allophane and imogolite. Soil Mineralogy with environmental applications, 7, 291–322. https://doi.org/10.2136/sssabookser7.c9

Hartge, K.H., Horn, R., 2016. Essential Soil Physics, an Introduction to Soil Processes, Functions, Structure and Mechanics. Schweizerbart science publishers.

Haas, C., Horn, R., Gerke, H.H., Dec, D., Zúñiga, F., Dörner, J., 2018. Air permeability and diffusivity of an Andisol subsoil as influenced by pasture improvement strategies. Agro Sur 46(2), 23–34. https://doi.org/10.4206/agrosur.2018.v46n2-05

Horn, R., 1988. Compressibility of arable land in Impact of water and external forces on soil structure. Selected papers of the 1st Workshop on soil physics and soil mechanics, Hannover 1986. Catena. Supplement (Giessen), (11), pp. 53–71.

Horn, R., Fleige, H., 2003. A method for assessing the impact of load on mechanical stability and on physical properties of soils. Soil Till. Res. 73(1-2), 89–99. https://doi.org/10.1016/S0167-1987(03)00102-8

Horn, R., Smucker, A., 2005. Structure formation and its consequences for gas and water transport in unsaturated arable and forest soils. Soil Till. Res. 82, 5–14. https://doi.org/10.1016/j.still.2005.01.002

Horn, R., Fleige, H., 2009. Risk assessment of subsoil compaction for arable soils in Northwest Germany at farm scale. Soil Till Res 102, 201–208. https://doi.org/10.1016/j.still.2008.07.015

Horn, R., Mordhorst, A., Fleige, H., 2021. Consequences of gas pipeline hauling on changes in soil properties over three years. Soil Till. Res. 211, 105002. https://doi.org/10.1016/j.still.2021.105002

Instituto Nacional de Estadísticas (INE), 2020. Informe anual 2019 medio ambiente, Región de Los Ríos. Edición Nº05/Junio de 2020, Valdivia, Chile.

Jones, R.J., Spoor, G., Thomasson, A.J., 2003. Vulnerability of subsoils in Europe to compaction: a preliminary analysis. Soil Till. Res. 73(1-2), 131–143. https://doi.org/10.1016/S0167-1987(03)00106-5

Keller, T., Colombi, T., Ruiz, S., Pogs Manalili, M., Rek, J., Stadelmann, V., Wunderli, H., Breitenstein, D., Reiser, R., Oberholzer, H., Schymanski, S., Romero-Ruiz, A., Linde, N., Weisskopf, P., Walter, A., Or, D., 2017. Long-Term Soil Structure Observatory for Monitoring Post-Compaction Evolution of Soil Structure. Vadose Zone J. 16(4), 1–16. https://doi.org/10.2136/vzj2016.11.0118

Keller, T., Sandin, M., Colombi, T., Horn, R., Or, D., 2019. Historical increase in agricultural machinery weights enhanced soil stress levels and adversely affected soil functioning. Soil Till Res. 194, 104293. https://doi.org/10.1016/j.still.2019.104293

Lal, R., 2015. Restoring soil quality to mitigate soil degradation. Sustainability 7(5), 5875-5895. https://doi.org/10.3390/su7055875

Lipiec, J., Hatano, R., 2003. Quantification of compaction effects on soil physical properties and crop growth. Geoderma 116(1-2), 107–136. https://doi.org/10.1016/S0016-7061(03)00097-1

Lipiec, J., Horn, R., Pietrusiewicz, J., Siczek, A., 2012. Effects of soil compaction on root elongation and anatomy of different cereal plant species. Soil Till. Res. 121, 74–81. https://doi.org/10.1016/j.still.2012.01.013

Lin, H., Horn, R., 2015. United Nations highlights soil crisis. Nature 517(7536), 553-553. https://doi.org/10.1038/517553d

Matus, F., Rumpel, C., Neculman, R., Panichini, M., Mora, M.L., 2014. Soil carbon storage and stabilisation in andic soils: A review. Catena 120, 102–110. https://doi.org/10.1016/j.catena.2014.04.008

Meurer, K., Barron, J., Chenu, C., Coucheney, E., Fielding, M., Hallett, P., Herrmann, A.M., Keller, T., Koestel, J., Larsbo, M. Lewan, E., 2020. A framework for modelling soil structure dynamics induced by biological activity. Glob. Change Biol. 26 (10), 5382–5403. https://doi.org/10.1111/gcb.15289

Mera, M., Lizana, X.C., Calderini, D.F., 2015. Cropping systems in environments with high yield potential of Southern Chile. In: Sadras, V.O., Calderini, D.F. (Eds.), Crop physiology-Applications for genetic improvement and agronomy (2nd ed.), Waltham, MA: Academic Press. pp. 111–140. https://doi.org/10.1016/B978-0-12-417104-6.00006-6

McQueen, D.J., Shepherd, T.G., 2002. Physical changes and compaction sensitivity of a fine-textured, poorly drained soil (Typic Endoaquept) under varying durations of cropping, Manawatu Region, New Zealand. Soil Till. Res. 63(3-4), 93–107. https://doi.org/10.1016/S0167-1987(01)00231-8

Mzuku, M., Khosla, R., Reich, R., Inman, D., Smith, F., MacDonald, L., 2005. Spatial variability of measured soil properties across site-specific management zones. Soil Sci. Soc. Am. J. 69, 1572–1579. https://doi.org/10.2136/sssaj2005.0062

Negron, M., López, I., Dörner, J., 2019. Consequences of intensive grazing by dairy cows of contrasting live weights on volcanic ash top soil structure and pasture dynamics. Soil Till. Res. 189, 88–97. https://doi.org/10.1016/j.still.2018.12.025

Nielsen, D.R., Wendroth, O., 2003. Spatial and temporal statistics: Sampling field soils and their vegetation. Catena Verlag, Reiskirchen, Germany.

Peth, S., Horn, R., 2006. The mechanical behavior of structured and homogenized soil under repeated loading. J. Plant Nutr. Soil Sci. 169, 401–410. https://doi.org/10.1002/jpln.200521942

Peth, S., J. Rostek, A. Zink, A. Mordhorst, Horn, R., 2010. Soil testing of dynamic deformation processes of arable soils. Soil Till. Res. 106, 317–328. https://doi.org/10.1016/j.still.2009.10.007

Pinochet, D., 2011. Guía para la fertilización de cultivos brássicas forrajeras. In: Cultivo y utilización de brássicas forrajeras en la Patagonia húmeda (Aysén). Hepp, C. (Ed.). Boletín INIA Nº 228. Coyhaique, Chile, pp.33–49.

Rabot, E., Wiesmeier, M., Schlüter, S., Vogel, H. J., 2018. Soil structure as an indicator of soil functions: A review. Geoderma 314, 122–137. https://doi.org/10.1016/j.geoderma.2017.11.009

Reszkowska, A., Krümmelbein, J., Zhao, Y., Peth, S., Horn, R., Gan, L., 2011. Influence of grazing on hydraulic and mechanical properties of semiarid steppe soils under different vegetation type in Inner Mongolia, China. Plant Soil 340, 59–72. https://doi.org/10.1007/s11104-010-0405-3

Reynolds, W.D., Drury, C.F., Tan, C.S., Fox, C.A., Yang, X.M., 2009. Use of indicators and pore volume-function characteristics to quantify soil physical quality. Geoderma 152(3-4), 252–263. https://doi.org/10.1016/j.geoderma.2009.06.009

R Core Team, 2020. R: A language and environment for statistical computing. R Foundation for Statistical Computing, Vienna, Austria. URL https://www.R-project.org/.

RStudio Team, 2020. RStudio: Integrated Development Environment for R. RStudio, PBC, Boston, MA. URL http://www.rstudio.com/

Salas, R., Ordóñez, I., Valle, S., López, I., Dec, D., Descalzi, C., Dörner, J., 2016. Variación espacial de propiedades físicas de un suelo derivado de cenizas volcánicas sometido a distintas estrategias de mejoramiento de una pradera degradada. Agro Sur 44(3), 29–40. https://doi.org/10.4206/agrosur.2016.v44n3-04

Seguel, O., Horn, R., 2006. Structure properties and pore dynamics in aggregate beds due to wetting–drying cycles. J. Plant Nutr. Soil Sci.169(2), 221–232. https://doi.org/10.1002/jpln.200521854

Simojoki, A., Fazekas-Becker, O., Horn, R., 2008. Macro-and microscale gaseous diffusion in a Stagnic Luvisol as affected by compaction and reduced tillage. Agric. Food Sci. 17(3), 252–264. https://doi.org/10.2137/145960608786118820

Soil Survey Staff, 2010. USDA-Natural Resources Conservation Services. Washington DC, 11th ed.

Solgi, A., Naghdi, R., Marchi, E., Laschi, A., Keivan Behjou, F., Hemmati, V., Masumian, A., 2019. Impact Assessment of Skidding Extraction: Effects on Physical and Chemical Properties of Forest Soils and on Maple Seedling Growing along the Skid Trail. Forests 10(2), 134. https://doi.org/10.3390/f10020134.

Schjønning, P., Rasmussen, K.J., 2000. Soil strength and soil pore characteristics for direct drilled and ploughed soils. Soil Till. Res. 57(1-2), 69–82. https://doi.org/10.1016/S0167-1987(00)00149-5

Shah, A.N., Tanveer, M., Shahzad, B., Yang, G., Fahad, S., Ali, S., Bukhari, M.A., Tung, S.A., Hafeez, A. Souliyanonh, B., 2017. Soil compaction effects on soil health and cropproductivity: an overview. Environ. Sci. Pollut. R. 24(11), 10056–10067. https://doi.org/10.1007/s11356-017-8421-y

Techen, A.K., Helming, K., Brüggemann, N., Veldkamp, E., Reinhold-Hurek, B., Lorenz, M., Bartke, S., Heinrich, U., Amelung, W., Augustin, K., Boy, J., 2020. Soil research challenges in response to emerging agricultural soil management practices. Adv. Agron. 161, 179–240. https://doi.org/10.1016/bs.agron.2020.01.002

Valle, S. R., Dörner, J., Zúñiga, F., Dec, D., 2018. Seasonal dynamics of the physical quality of volcanic ash soils under different land uses in southern Chile. Soil Till. Res. 182, 25–34. https://doi.org/10.1016/j.still.2018.04.018

Vásquez, N., Salazar, F., Dörner, J., 2012. Variabilidad temporal de las propiedades físico-mecánicas de un suelo derivado de cenizas volcánicas bajo labranza convencional. Agro Sur 40(3), 1–13. https://doi.org/10.4206/agrosur.2012.v40n3-01

Wendroth, O., Koszinski, S., Vasquez, V., Huang, P.M., Li, Y., Sumner, M.E., 2011. Soil spatial variability. Handbook of soil sciences properties and processes. 2nd ed. CRC Press, Boca Raton, FL. p, 10(10.25).

WRB., 2006. World reference base for soil resources. 2nd edition. World Soil Resources Reports No. 103. FAO, Rome. 145 p.

Zúñiga, F., Ivelic-Sáez, J., López, I., Huygens, D., Dörner, J., 2015. Temporal dynamics of the physical quality of an Andisol under a grazing system subjected to different pasture improvement strategies. Soil Till Res. 145, 233–241. https://doi.org/10.1016/j.still.2014.09.014

Zúñiga, F., Horn, R., Rostek, J., Peth, S., Uteau, D., Dörner, J., 2019. Anisotropy of intensity–capacity parameters on Aquands with contrasting swelling–shrinkage cycles. Soil Till. Res. 193, 101–113. https://doi.org/10.1016/j.still.2019.05.019

Table headings

Table 1. Descriptive statistics of field physical properties measured in July (05.07.19) in the studied volcanic ash soil.

Table 2. Geostatistical parameters of field physical properties measured in July (05.07.19) in the studied volcanic ash soil.

Table 1 Descriptive statistics of field physical properties measured in July (05.07.19) in the studied volcanic ash soil.

SPP	WC [Vol. %]	PR [MPa]	Kl [cm s^{-1}]	$PR_{0\text{-}5cm}$ [MPa]	$PR_{0\text{-}20cm}$ [MPa]	$PR_{0\text{-}60cm}$ [MPa]
N	94	96	96	96	96	96
Mean	50	0.75	2.44	4.6	26.8	75.1
Median	52	0.70	0.96	4.7	27.5	74.3
CV	12	42	148	35	15	11
Min.	32	0.20	0.03	1.0	12.7	58.7
Max.	61	1.50	17.60	7.8	34.3	96.0
Skewness	-0.91	0.23	-0.13	-0.25	-0.58	0.40
Kurtosis	0.48	-0.44	-0.93	-0.70	0.39	-0.39

SPP = Soil physical property; WC = Volumetric water content; PR = Penetration resistance; Kl = Air conductivity. $PR_{0\text{-}5cm}$, $PR_{0\text{-}20cm}$ and $PR_{0\text{-}60\ cm}$ represents the cumulative PR values between 0–5 cm, 0–20 cm and 0–60 cm, respectively. Skewness and Kurtosis parameters correspond to the log-transformed Kl data.

Table 2 Geostatistical parameters of field physical properties measured in July (05.07.19) in the studied volcanic ash soil.

SPP	WC	PR	Kl	$PR_{0\text{-}5cm}$	$PR_{0\text{-}20cm}$	$PR_{0\text{-}60cm}$
Model	Gaussian	Exponential	Exponential	Spherical	Exponential	Exponential
Co	21.9	0.046	1.49	1.108	10.25	34.6
Co + C	72.8	0.192	3.829	3.798	33.82	120.2
Ao [m]	107.7	303.0	89.8	101	303.0	213.8
R^2	0.68	0.72	0.82	0.76	0.615	0.82
RSS	236	9.4×10^{-4}	0.534	0.78	38.6	294
DD	30	24	38	29	30	29
A [m]	107.7	303	89.8	101	303.3	213.8

SPP = Soil physical property; WC = Volumetric water content; PR = Penetration resistance; Kl = Air conductivity. $PR_{0\text{-}5cm}$, $PR_{0\text{-}20cm}$ and $PR_{0\text{-}60\ cm}$ represents the cumulative PR values between 0–5 cm, 0–20 cm and 0–60 cm, respectively. Co = Nugget; Co + C = Sill; Ao = Model range parameters; RSS = Residual sum of squares; DD = Dependence degree; A = Range.

Figure captions

Figure 1. Air temperature and precipitation during 2019. Data was downloaded from AGROMET (https://www.agromet.cl) using the weather station located in the Estación Experimental Agropecuaria Austral (1.5 km from the experiment). Dates of field measurements (M) and soil samplings (SS) are included.

Figure 2. Schematic representation of soil tillage, homogenization and compaction. The soil tillage and homogenization were conducted using offset (5 times) and tandem (1) discs. Thereafter, a Roller (1.20 Mg) completed the homogenization of all blocks (1 pass) and the first field measurement was conducted (M1). Penetration resistance (PR) and field volumetric water content (θ_{Field}) measurements (M1, M2, M3 and M4) were conducted after the soil compaction events (SCE) applied to reach the different soil bulk densities.

Figure 3. Temporal changes in penetration resistance (PR, A) and field volumetric water content (θ_{Field}, B) due to soil tillage and soil compaction events (SCE) during pasture establishment. Mean values ± 1 standard error are presented (n=10). T0: 0.65 Mg m^{-3}, T1: 0.75 Mg m^{-3} and T3: 0.85 Mg m^{-3}. In PR red and blue dashed lines indicate PR values measured in the same soil under an intensively grazed pasture and directly after soil tillage. The dashed lines in θ_{Field} indicate the volumetric water contents at field capacity (pF 1.78) and permanent wilting point (pF 4.18). Different lowercase letters indicate significant differences in the PR and θ_{Field} among soil compaction events ($p \leq 0.05$). Furthermore, there was an interaction between roller compaction events and treatments for θ_{Field} ($p < 0.001$). There was no significant interaction among treatments ($p > 0.05$). The grey area emphasizes that these field measurements were conducted the same day.

Figure 4. Spatial variability of penetration resistance (PR, A) measured at the 10 cm depth, field volumetric water content (WC, B) and air conductivity (Kl, C), measured in July (05.07.19).

Figure 5. Spatial variability of penetration resistance (PR, measured in 05.07.19): A, B and C show the cumulative PR values between 0–5 cm, 0–20 cm and 0–60 cm, respectively.

Figure 6. Penetration resistance profiles at field (A and B) and cylinder (C) scales. A shows PR values measured with 1 cm of separation from soil surface till the 80 cm depth, while B presents the cumulative PR values till the same soil depth. C represents PR values measured in cylinders collected at the soil surface and the 20 cm depth. T0: 0.65 Mg m^{-3}, T1: 0.75 Mg m^{-3} and T3: 0.85

Mg m^{-3}. The photo shows the platy soil structure formed after roller compaction in T2. Furthermore, the accumulated penetration resistance (APR) is presented for each compaction level evaluated at depths of 10, 20 and 60 cm (D). Different lowercase letters indicate significant interaction of the factors depth (10, 20 and 60 cm) and accumulated penetration resistance ($p<0.001$).

Figure 7. Temporal changes in bulk density (Bd, A), precompression stress (Pc, B), plant available water (PAW, C), air capacity (AC, D) and air permeability before (Ka BCE, E) and after (Ka ACE, F) the consolidation experiment. Mean values ± 1 standard error are presented (n = 6). Furthermore, the interaction between date and treatments was observed for Bd, Pc and wCP and was indicated with lowercase letters ($p \leq 0.05$). For plots without interaction (PAW, Ka BCF and Ka ACF), uppercase letters indicate differences among sampling dates (15.05.2019, 16.06.2019 and 17.09.2019; $p \leq 0.05$) and lowercase letters indicate differences among treatments (T0: 0.65 Mg m^{-3}, T1: 0.75 Mg m^{-3} and T3: 0.85 Mg m^{-3}; $p \leq 0.05$).

Figure 8. Precompression stress (Pc, A), plant available water (PAW, B), air capacity (AC, C) and air permeability (Ka, D) as a function of bulk density. Red lines present critical values concerning soil compaction for AC (Reynolds et al., 2009) and Ka (Ball et al., 1988) and a classification of Pc values according to Horn and Fleige (2003).

Figure 9. Plant available water (PAW, A), air permeability (Ka, B) and precompression stress (Pc, C) as functions of air capacity (AC). Red lines present critical values concerning soil compaction for AC (Reynolds et al., 2009) and Ka (Ball et al., 1988) and a classification of Pc values according to Horn and Fleige (2003).

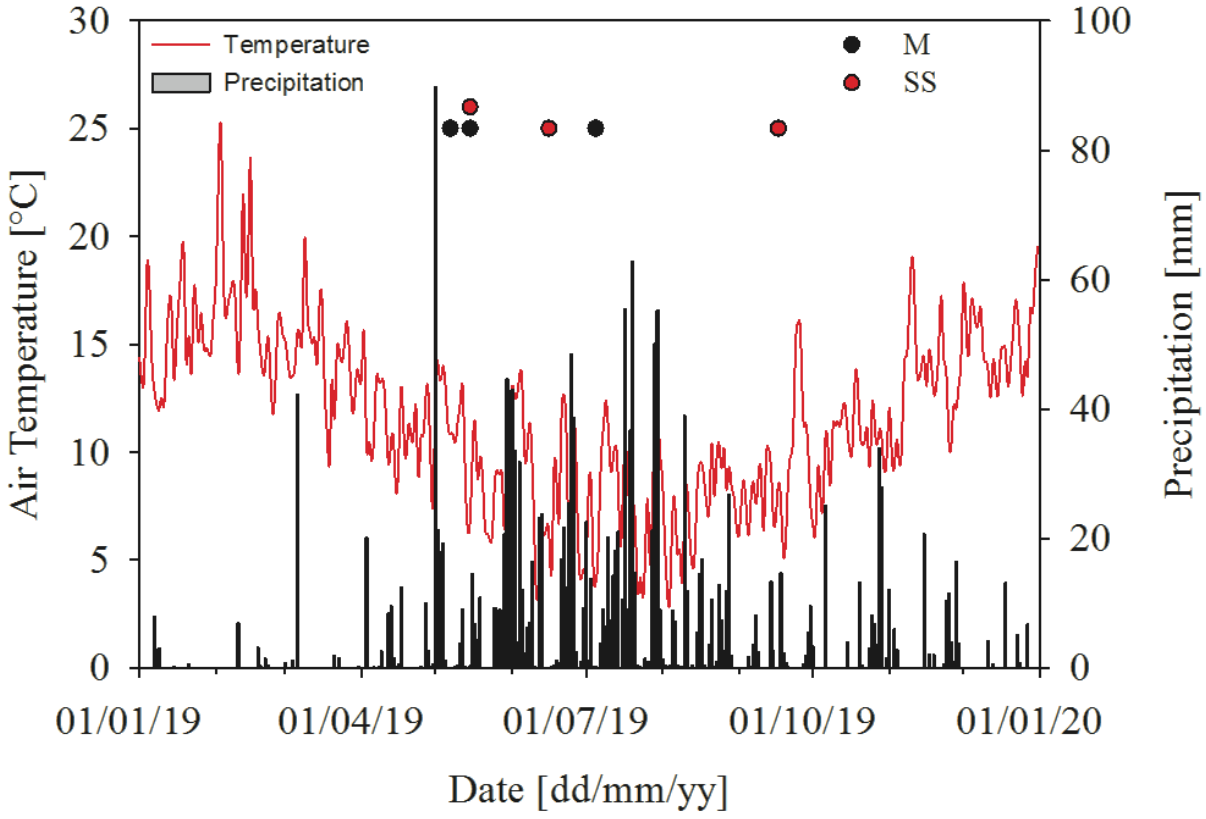
Temperature
Precipitation
M
SS
Air Temperature [°C]
Precipitation [mm]
Date [dd/mm/yy]
01/01/19
01/04/19
01/07/19
01/10/19
01/01/20
0
5
10
15
20
25
30
0
20
40
60
80
100

Figure 1


Date 1
May 7th 2019
Date 2
May 14th 2019
Date 3
May 15th 2019
Soil Tillage, Homogenization and Compaction 1
T0: Roller (1P; M1) | Sowing | Roller (1P; M2)
T1: Roller (1P; M1) | Güttler (1P) | Roller (1P) | Sowing | Roller (1P; M2)
T2: Roller (1P; M1) | Roller (3P) | Güttler (3P) | Roller (1P) | Sowing | Roller (1P; M2)
M1 and M2: PR and θField measurements after first and second Soil Compaction Event (SCE), respectively.
Compaction 2
T0: (-; M3)
T1: Roller (2P; M3)
T2: Roller (5P; M3)
M3: PR and θField measerements after defined SCE.
Compaction 3
T0: (-; M4)
T1: (-; M4)
T2: Roller (2P; M4)
M4: PR and θField measurements after defined SCE.
T0 = 0.65 Mg m-3
T1 = 0.75 Mg m-3
T2 = 0.85 Mg m-3
Not compacted
Compacted
Highly Compacted

Figure 2

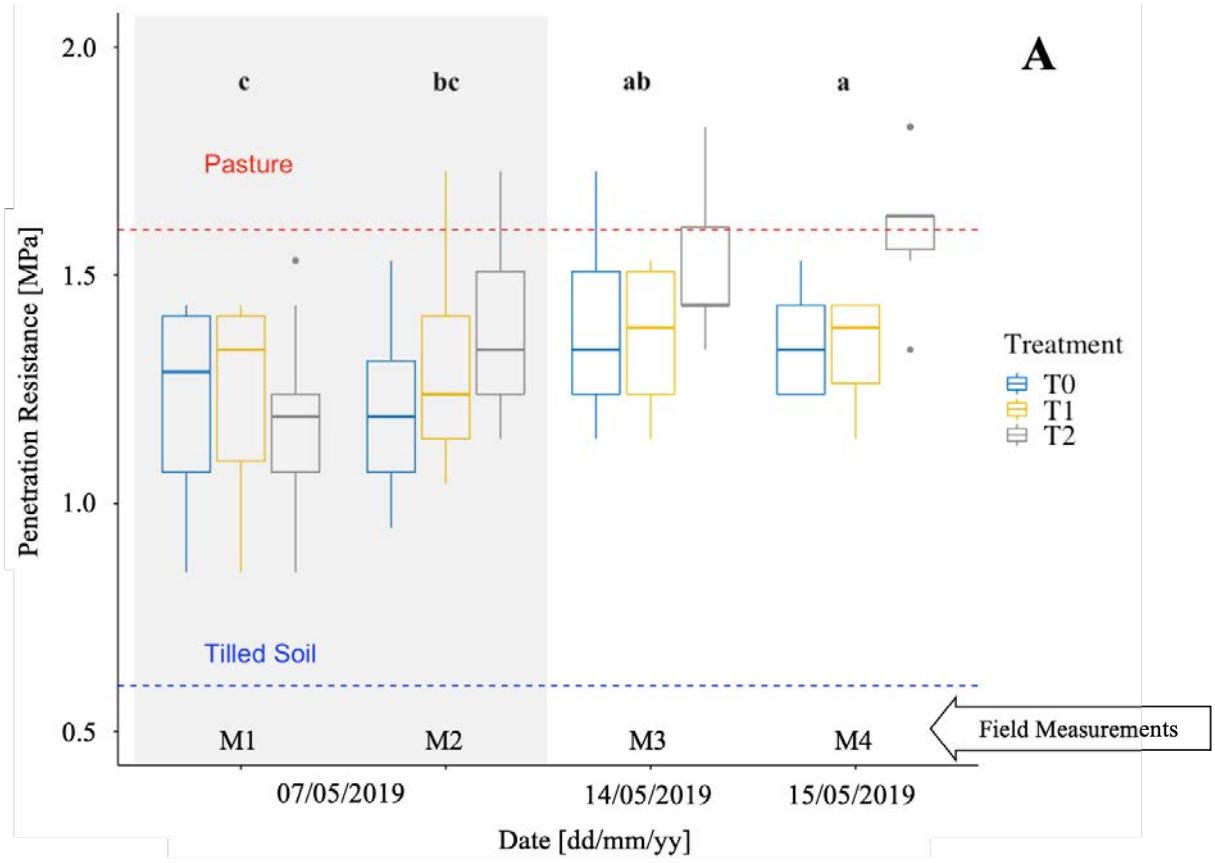
A
2.0
1.5
1.0
0.5
Penetration Resistance [MPa]
c
bc
ab
a
Pasture
Tilled Soil
Treatment
T0
T1
T2
M1
M2
M3
M4
Field Measurements
07/05/2019
14/05/2019
15/05/2019
Date [dd/mm/yy]

1

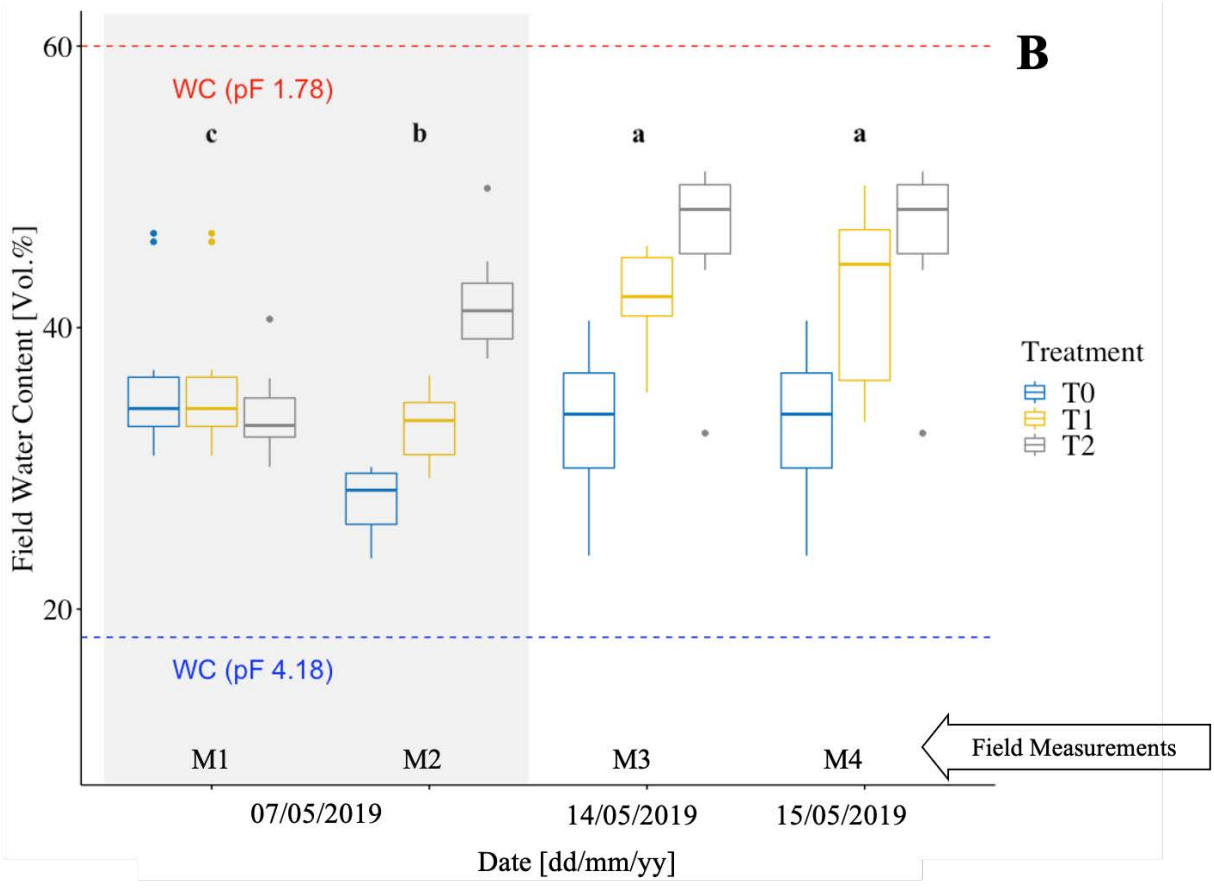
B
60
40
20
Field Water Content [Vol.%]
WC (pF 1.78)
WC (pF 4.18)
c
b
a
a
Treatment
T0
T1
T2
M1
M2
M3
M4
Field Measurements
07/05/2019
14/05/2019
15/05/2019
Date [dd/mm/yy]

2

3 Figure 3

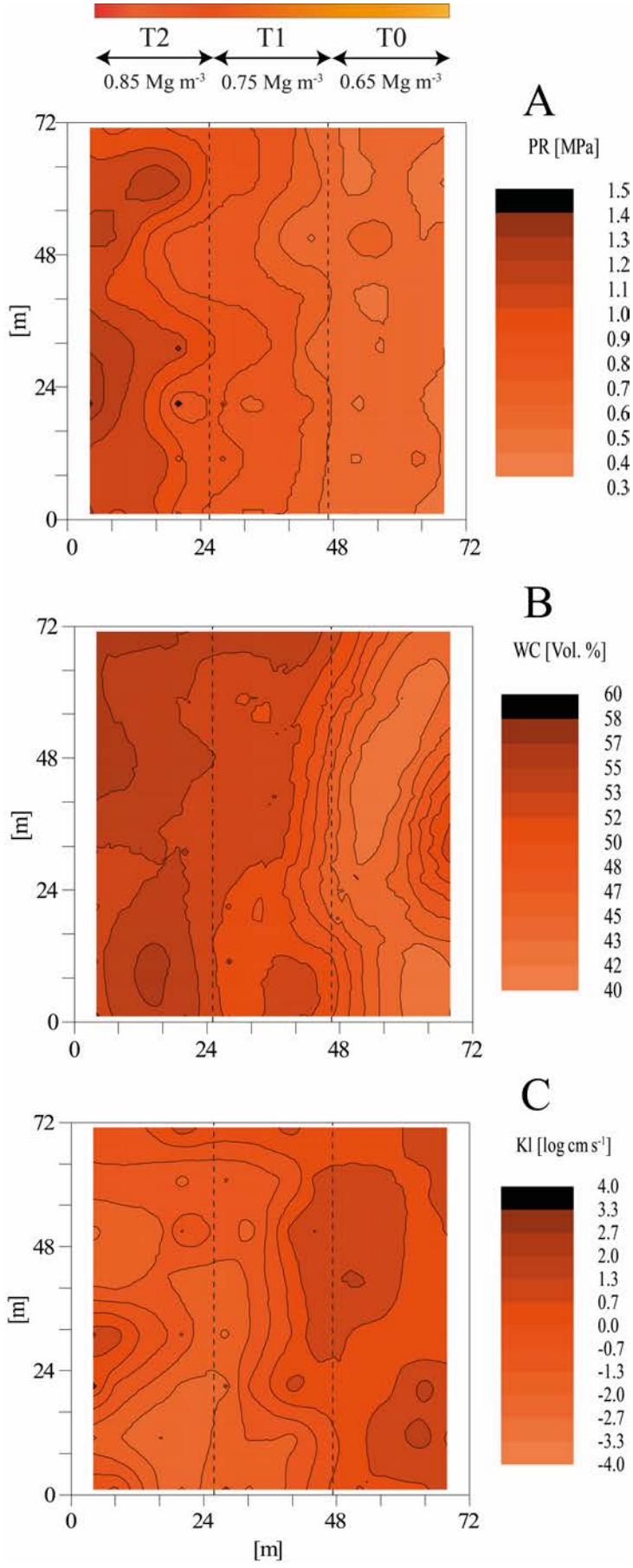
T2
T1
T0
0.85 Mg m-3
0.75 Mg m-3
0.65 Mg m-3
A
PR [MPa]
1.5
1.4
1.3
1.2
1.1
1.0
0.9
0.8
0.7
0.6
0.5
0.4
0.3
B
WC [Vol. %]
60
58
57
55
53
52
50
48
47
45
43
42
40
C
Kl [log cm s-1]
4.0
3.3
2.7
2.0
1.3
0.7
0.0
-0.7
-1.3
-2.0
-2.7
-3.3
-4.0
[m]
0
24
48
72

Figure 4

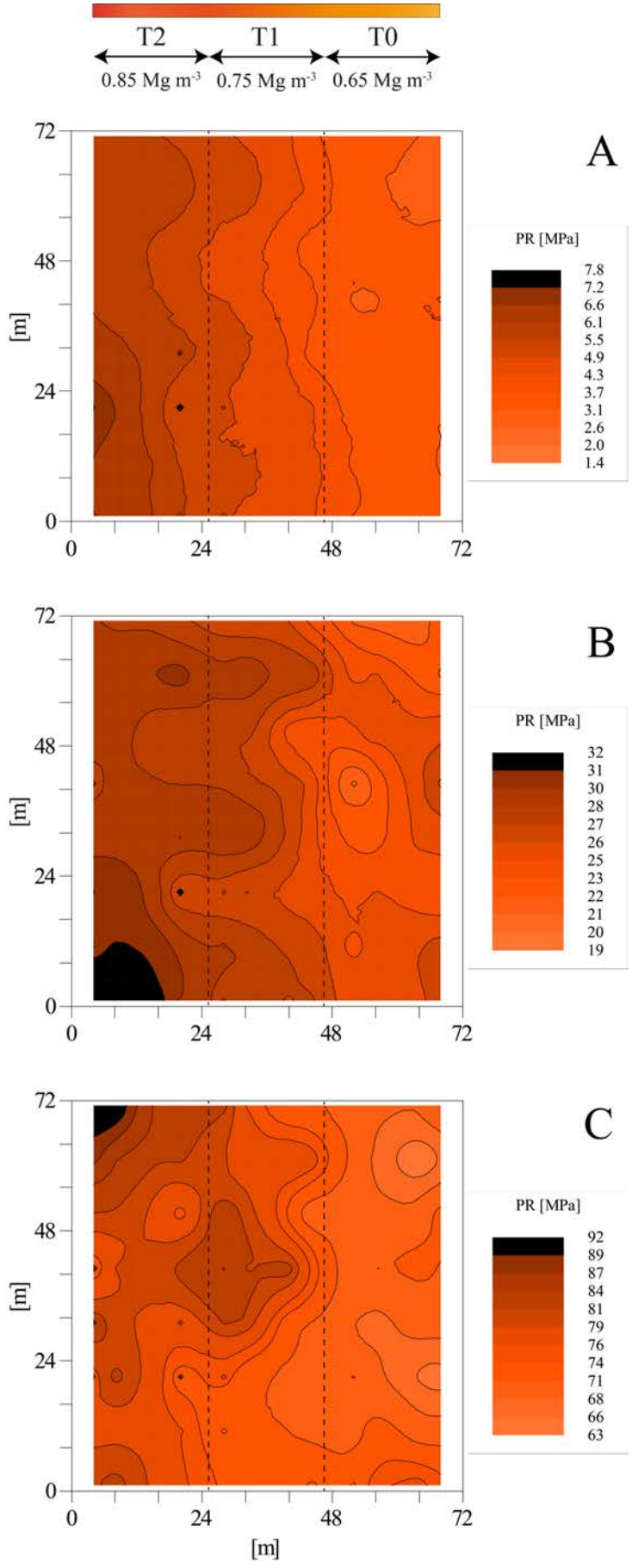
T2
T1
T0
0.85 Mg m-3
0.75 Mg m-3
0.65 Mg m-3
A
PR [MPa]
7.8
7.2
6.6
6.1
5.5
4.9
4.3
3.7
3.1
2.6
2.0
1.4
B
PR [MPa]
32
31
30
28
27
26
25
23
22
21
20
19
C
PR [MPa]
92
89
87
84
81
79
76
74
71
68
66
63
[m]
0
24
48
72

Figure 5

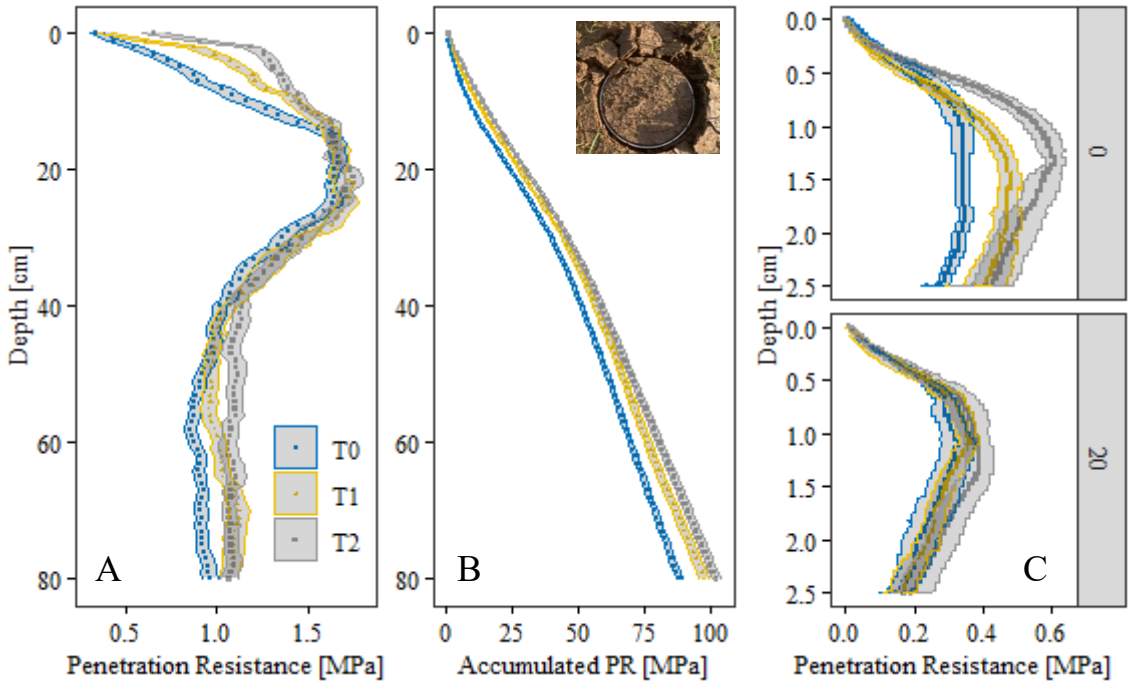
Depth [cm]
Penetration Resistance [MPa]
T0
T1
T2
A
Accumulated PR [MPa]
B
C
0
20

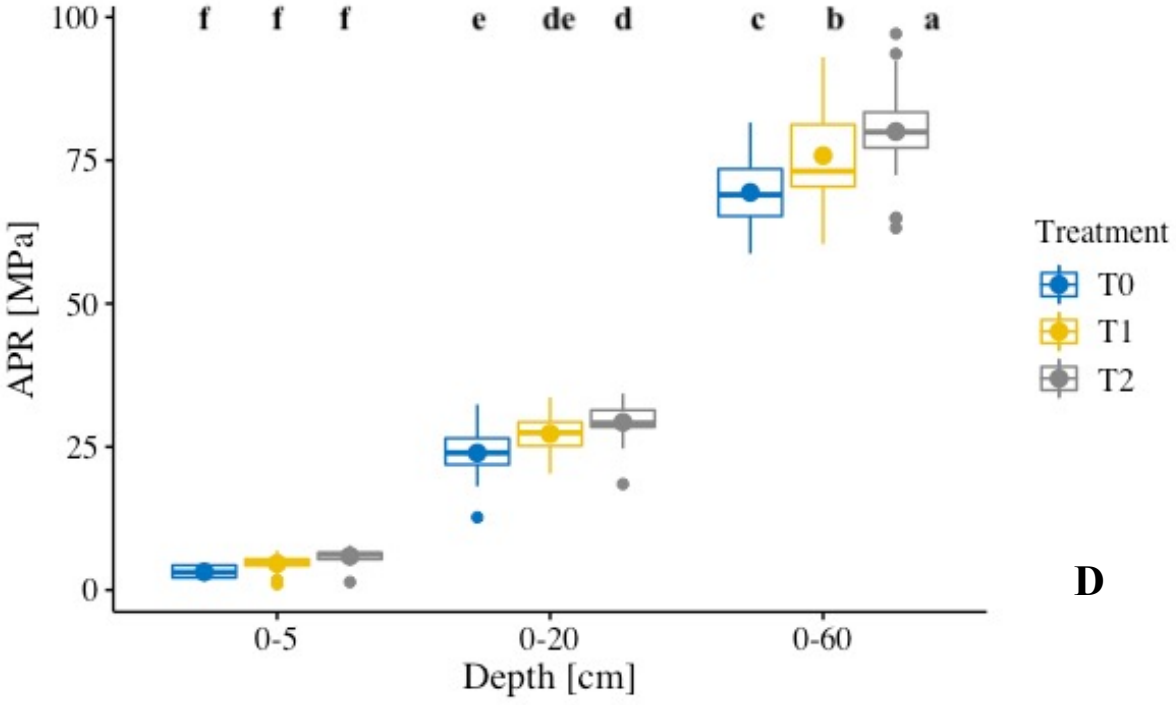
APR [MPa]
f f f e de d c b a
Treatment
T0
T1
T2
0-5
0-20
0-60
Depth [cm]
D

Figure 6

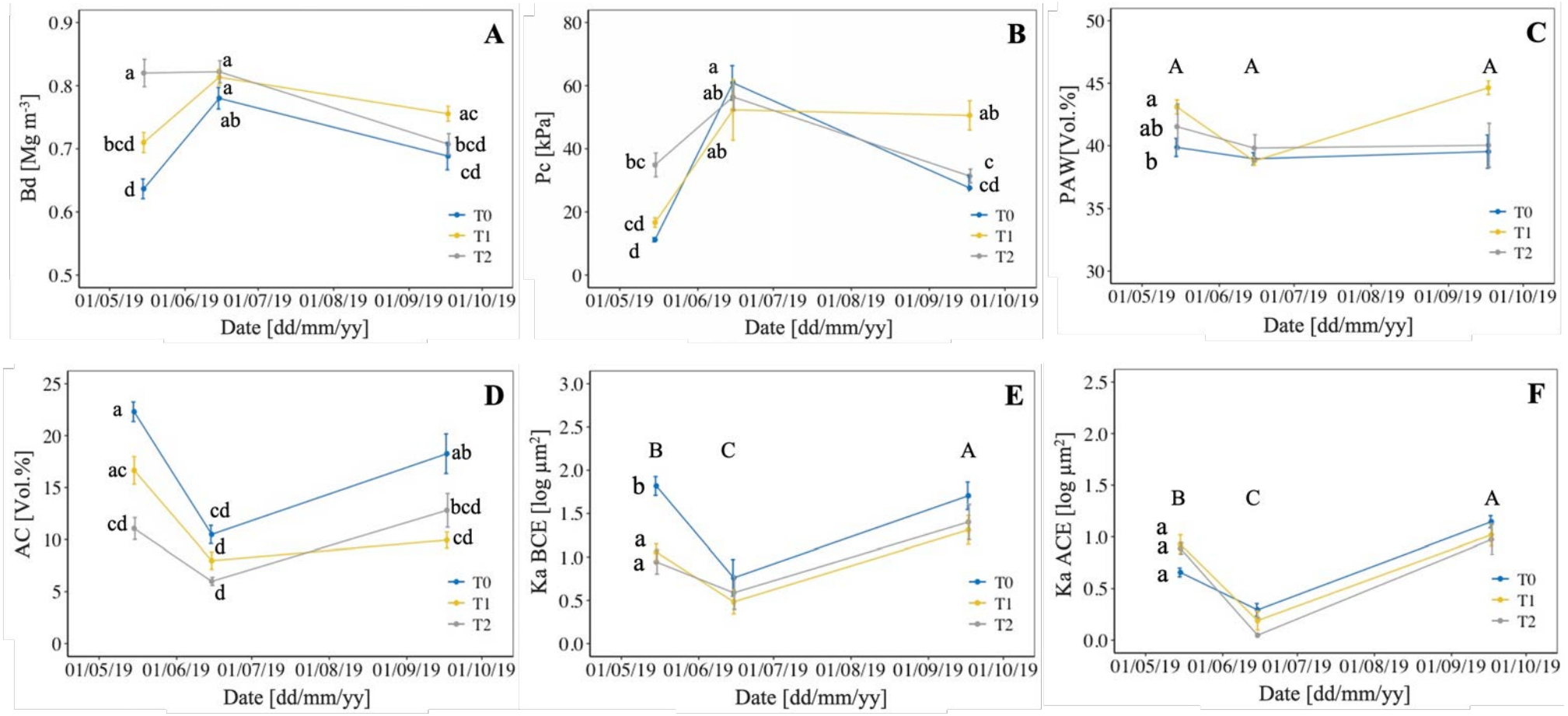
A
Bd [Mg m-3]
Date [dd/mm/yy]
01/05/19 01/06/19 01/07/19 01/08/19 01/09/19 01/10/19
T0
T1
T2
B
Pc [kPa]
C
PAW[Vol.%]
D
AC [Vol.%]
E
Ka BCE [log µm2]
F
Ka ACE [log µm2]

Figure 7

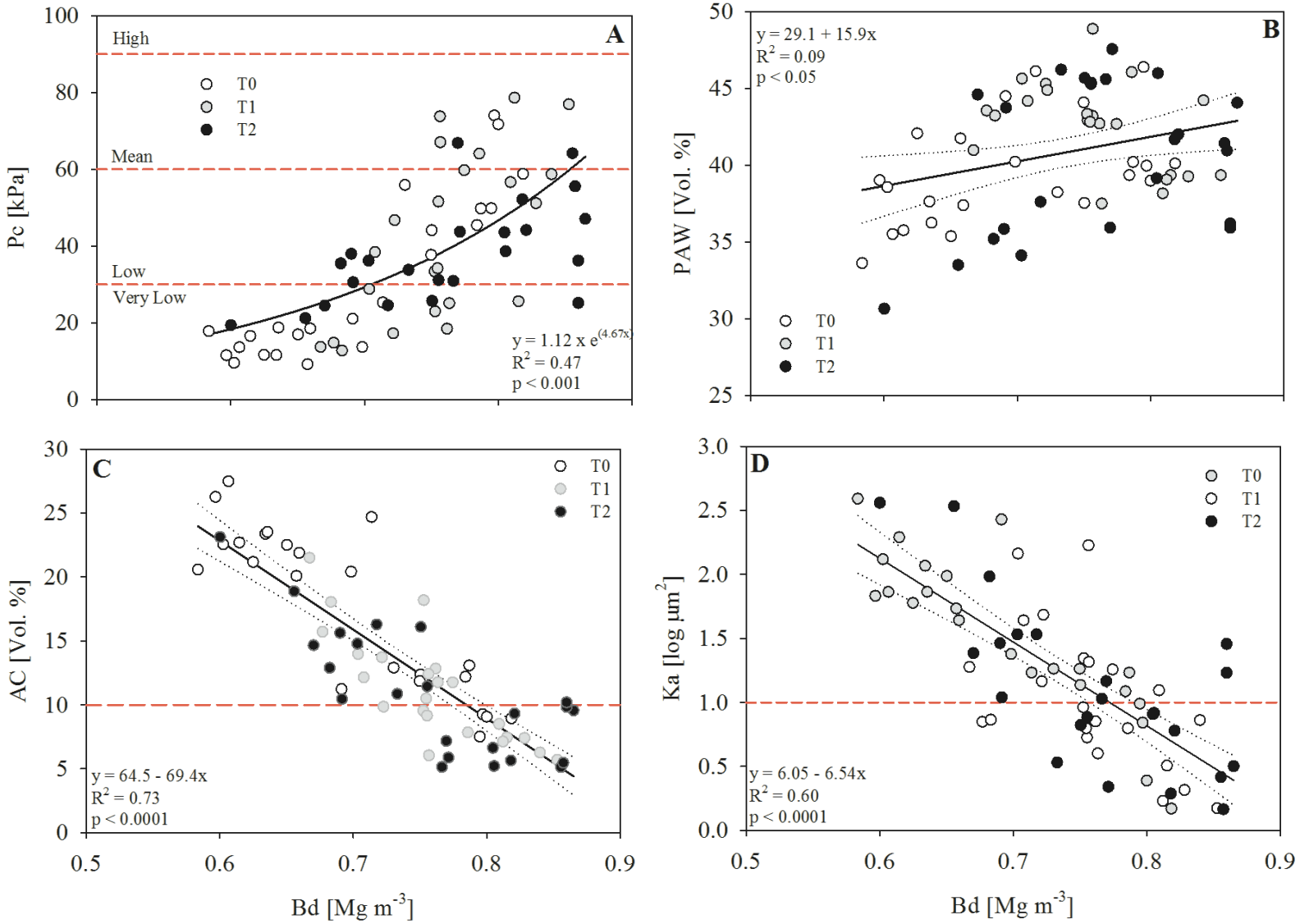
A
High
Mean
Low
Very Low
T0
T1
T2
Pc [kPa]
y = 1.12 x e(4.67x)
R2 = 0.47
p < 0.001
B
y = 29.1 + 15.9x
R2 = 0.09
p < 0.05
PAW [Vol. %]
C
AC [Vol. %]
y = 64.5 - 69.4x
R2 = 0.73
p < 0.0001
Bd [Mg m-3]
D
Ka [log µm2]
y = 6.05 - 6.54x
R2 = 0.60
p < 0.0001
Bd [Mg m-3]

Figure 8

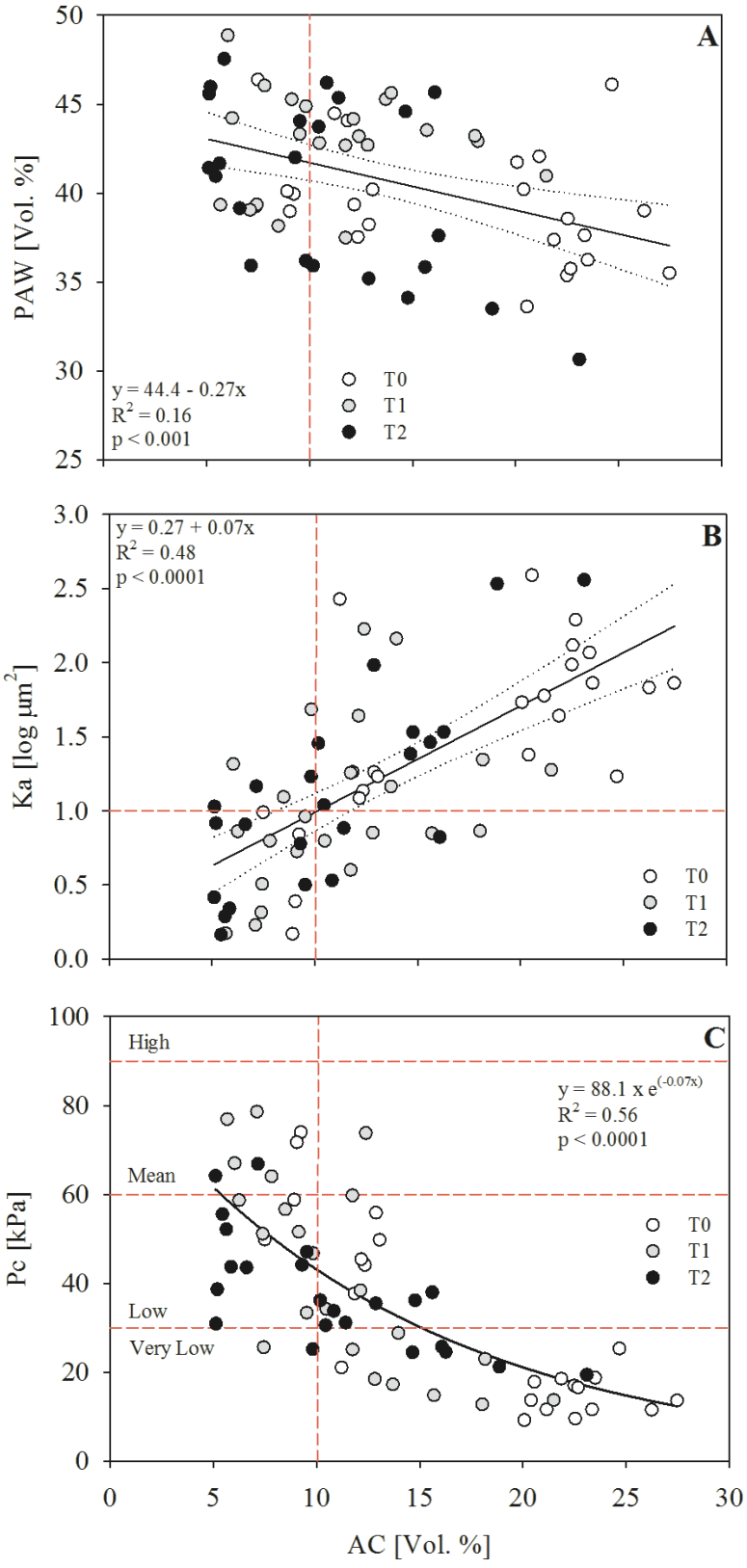
A
PAW [Vol. %]
y = 44.4 - 0.27x
R² = 0.16
p < 0.001
T0
T1
T2
B
Ka [log µm²]
y = 0.27 + 0.07x
R² = 0.48
p < 0.0001
C
Pc [kPa]
High
Mean
Low
Very Low
y = 88.1 x e^(-0.07x)
R² = 0.56
p < 0.0001
AC [Vol. %]

Figure 9

1

2

3